

Neutron-Inelastic-Scattering Peak by Dissipationless Mechanism in the s_{++} -wave State in Iron-based Superconductors

Seiichiro ONARI¹ and Hiroshi KONTANI²

¹ Department of Applied Physics, Nagoya University and JST, TRIP, Furo-cho, Nagoya 464-8602, Japan.

² Department of Physics, Nagoya University and JST, TRIP, Furo-cho, Nagoya 464-8602, Japan.

(Dated: November 12, 2018)

We investigate the neutron scattering spectrum in iron pnictides based on the random-phase approximation in the five-orbital model with a realistic superconducting (SC) gap, $\Delta = 5\text{meV}$. In the normal state, the neutron spectrum is suppressed by large inelastic quasi-particle (QP) scattering rate $\gamma^* \sim \Delta$. In the fully-gapped s -wave state without sign reversal (s_{++}), a hump-shaped enhancement appears in the neutron spectrum just above 2Δ , since the inelastic QP scattering is prohibited by the SC gap. That is, the hump structure is produced by the dissipationless QPs for QP energy $E_{\mathbf{k}} < 3\Delta$. The obtained result is more consistent with experimental spectra, compared to the results of our previous paper with $\Delta = 50\text{meV}$. On the other hand, both height and weight of the resonance peak in the fully-gapped s -wave states with sign reversal (s_{\pm}) are much larger than those observed in experiments. We conclude that experimentally observed broad spectral peak in iron pnictides is created by the present “dissipationless mechanism” in the s_{++} -wave state.

PACS numbers: 74.20.-z, 74.20.Rp, 78.70.Nx

I. INTRODUCTION

Since the discovery of superconductivity in iron pnictides with high transition temperature (T_c)¹, substantial experimental and theoretical works have been performed to clarify the mechanism of superconductivity. The superconducting (SC) gap in many iron pnictides is fully-gapped and band-dependent, as shown by the penetration depth measurement² and the angle-resolved photoemission spectroscopy (ARPES)^{3,4}. The fully-gapped state is also supported by the rapid suppression in $1/T_1$ ($\propto T^n$; $n \sim 4 - 6$) below T_c ⁵⁻⁷. On the other hand, P-doped Ba122⁸ and LaFePO^{9,10} show the nodal line behavior (T -linear dependence) in penetration depth measurements. In these compounds, A_{1g} symmetry pairing states with accidental nodes are expected theoretically.^{11,12}

In iron pnictides, the intra-orbital nesting of the Fermi surface (FS) between the hole- and electron-pockets is expected to induce the antiferromagnetic (AF) fluctuations. Taking this fact into account, the fully-gapped sign-reversing s -wave state (s_{\pm} -wave state) mediated by the AF fluctuation had been predicted^{13,14}. On the other hand, we have demonstrated that the orbital fluctuation mediated fully-gapped s -wave state without sign-reversal (s_{++} -wave state) is realized by the inter-orbital nesting, by taking the electron-phonon interaction into account.^{15,16} In the latter scenario, the close relation between T_c and the crystal structure revealed by Lee¹⁷, *e.g.*, T_c becomes the highest when the As₄ cluster is regular tetrahedron, is automatically explained¹⁶. Moreover, the latter scenario is consistent with the large SC gap on the z^2 -orbital band in Ba122 systems¹⁶, observed by bulk-sensitive laser ARPES measurement¹⁸. In addition, the orthorhombic structure transition and the corresponding shear modulus softening is well explained theoretically¹⁹. In newly discovered $K_x\text{Fe}_2\text{Se}_2$

with $T_c \sim 30\text{K}$, in which only electron-pockets exist, orbital-fluctuation-mediated fully-gapped s_{++} -wave state²⁰ or spin-fluctuation-mediated nodal $d_{x^2-y^2}$ -wave state^{20,21} had been predicted theoretically.

Thus, it is important to clarify the sign of the SC gap via phase-sensitive experiments. Nonmagnetic impurity effect offers us useful phase-sensitive information. In iron pnictides, the SC state survives against high substitution of Fe sites by other element (more than 10%).²²⁻²⁵ These results support the s_{++} -wave state since the s_{\pm} -wave state is very fragile against impurities, similar to other unconventional superconductors.^{26,27} Moreover, impurity driven crossover from s_{\pm} -wave state to s_{++} -wave state had been discussed in Refs.^{12,21}.

Another promising method is the neutron scattering measurement: As discussed by Monthoux and Scalapino in Ref.²⁸, existence of the resonance peak at a nesting wavevector \mathbf{Q} is a strong evidence for AF fluctuation mediated superconductors with sign reversal²⁸⁻³¹. The resonance occurs under the condition $\omega_{\text{res}} < 2\Delta$, where ω_{res} is the resonance energy and Δ is magnitude of the SC gap. The sharp and large resonance peak has been observed in many AF fluctuation mediated unconventional superconductors, like high- T_c cuprates³²⁻³⁴, CeCoIn₅³⁵, and UPd₂Al₃³⁶. The measurements of phonon spectral function for $|\omega| \lesssim 2\Delta$ would also be useful.³⁷

Neutron scattering measurements for iron pnictides had been performed³⁸⁻⁴³ after the theoretical predictions^{44,45}. Although clear peak structures were observed in FeSe_{0.4}Te_{0.6}³⁹, BaFe_{2-x}Co_xAs₂^{40,42} and Ca-Fe-Pt-As⁴³, these weights are much smaller than those in high- T_c cuprates and CeCoIn₅. Moreover, the resonance condition $\omega_{\text{res}} < 2\Delta$ is not surely confirmed since it is difficult to determine the value of Δ accurately. For example in BaFe_{1.85}Co_{0.15}As₂, ω_{res} is observed as 10meV in neutron scattering measurement.⁴⁰ In this material, $2\Delta = \Delta_h + \Delta_e$, where $\Delta_{h(e)}$ denotes magnitude of gap

on the hole (electron) pocket. It was estimated as 11meV according to an earlier ARPES measurement.⁴⁶ However, $\Delta_h + \Delta_e$ was estimated as 7meV by a recent measurement of the specific heat⁴⁷. We also obtain $\Delta_h + \Delta_e = 7\text{meV}$ from a recent penetration depth measurement in Ref.⁴⁸, by the linear interpolation for $x = 0.14$ and $x = 0.17$.

In our previous paper⁴⁹, we revealed that for $\Delta = 50\text{meV}$ a prominent hump structure *free from the resonance mechanism* appears in neutron scattering spectrum just above 2Δ in the s_{++} -wave state. The hump structure originates from the dissipationless quasi-particles (QPs) free from the inelastic scattering in the SC state. Although the broad spectral peak observed in iron pnictides was naturally reproduced based on the s_{++} -wave state, rather than the s_{\pm} -wave state, used model parameters were not realistic.

In this paper, we investigate the dynamical spin susceptibility $\chi^s(\omega, \mathbf{Q})$ based on the five-orbital model¹³ for both s_{++} - and s_{\pm} -wave states, by improving the method of numerical calculation. Using a realistic parameter $\Delta = 5\text{meV}$, the obtained results are more realistic than our previous results for $\Delta = 50\text{meV}$.⁴⁹ In the normal state, $\chi^s(\omega, \mathbf{Q})$ is strongly suppressed by the inelastic QP damping γ^* , which is large due to the strong correlation. However, this suppression is released in the SC state since the inelastic damping γ^* disappears for $|\omega| \lesssim 3\Delta$. This “dissipationless mechanism” induces a hump-shaped enhancement in $\chi^s(\omega, \mathbf{Q})$ in the s_{++} -wave state, just above 2Δ till $\sim 3\Delta$. In the s_{\pm} -wave state, very high and sharp resonance peak appears at $\omega_{\text{res}} < 2\Delta$ even in the case of $\Delta = 5\text{meV}$. We demonstrate that the broad spectral peak observed in iron pnictides is naturally reproduced based on the s_{++} -wave state, rather than the s_{\pm} -wave state.

In Sec. III.C, we comment that Nagai *et al.*⁵⁰ fail to reproduce the spectral gap in the two-particle Green function 2Δ and are therefore unreliable. In appendix, we introduce the similar hump structure of the neutron scattering spectrum in CeNiSn much below the Kondo temperature T_K . This compound is called Kondo semiconductor since the hybridization gap Δ opens much below T_K , while it is an incoherent metal with large inelastic scattering above T_K . This is another example of the hump structure by the “dissipationless mechanism”, since the inelastic scattering is prohibited by the singlet gap Δ .

We note that numerical results are improved from results in the first version of preprint⁵¹, in which the value of $\gamma^*(\epsilon)$ for $3\Delta < \epsilon < 4\Delta$ was incorrect in our previous numerical calculation.

II. FORMULATION

A. Method of calculation

Now, we study the 10×10 Nambu BCS Hamiltonian $\hat{\mathcal{H}}_{\mathbf{k}}$ composed of the five-orbital tight-binding model and

the band-diagonal SC gap introduced in ref.²⁶. Then, the 10×10 Green function is given by

$$\begin{aligned} \hat{\mathcal{G}}(i\omega_n, \mathbf{k}) &\equiv \begin{pmatrix} \hat{G}(i\omega_n, \mathbf{k}) & \hat{F}(i\omega_n, \mathbf{k}) \\ \hat{F}^\dagger(i\omega_n, \mathbf{k}) & -\hat{G}(-i\omega_n, \mathbf{k}) \end{pmatrix} \\ &= (i\omega_n \hat{1} - \hat{\Sigma}_{\mathbf{k}}(i\omega_n) - \hat{\mathcal{H}}_{\mathbf{k}})^{-1}, \end{aligned} \quad (1)$$

where $\omega_n = \pi T(2n + 1)$ is the fermion Matsubara frequency, \hat{G} (\hat{F}) is the 5×5 normal (anomalous) Green function, and $\hat{\Sigma}_{\mathbf{k}}$ is the self-energy in the d -orbital basis. In this paper, we assume that the magnitude of the SC gap is band-independent; $|\Delta^\nu| = \Delta$.

Here, we have to calculate the spin susceptibility as function of real frequency. Numerically, it is rather easy to use the Matsubara frequency method and the numerical analytic continuation (pade approximation).^{44,45} In the present study, however, we perform the analytical continuation before numerical calculation in order to obtain more reliable results. The irreducible spin susceptibility in the singlet SC state is given by³¹

$$\begin{aligned} \hat{\chi}_{l_1 l_2, l_3 l_4}^{\text{OR}}(\omega, \mathbf{q}) &= \frac{1}{N} \sum_{\mathbf{k}} \int \frac{dx}{2} \\ &\left[\tanh \frac{x}{2T} G_{l_1 l_3}^{\text{R}}(x_+, \mathbf{k}_+) \rho_{l_4 l_2}^{\text{G}}(x, \mathbf{k}) \right. \\ &+ \tanh \frac{x_+}{2T} \rho_{l_1 l_3}^{\text{G}}(x_+, \mathbf{k}_+) G_{l_4 l_2}^{\text{A}}(x, \mathbf{k}) \\ &+ \tanh \frac{x}{2T} F_{l_1 l_4}^{\text{R}}(x_+, \mathbf{k}_+) \rho_{l_3 l_2}^{\text{F}\dagger}(x, \mathbf{k}) \\ &\left. + \tanh \frac{x_+}{2T} \rho_{l_1 l_4}^{\text{F}}(x_+, \mathbf{k}_+) F_{l_3 l_2}^{\dagger \text{A}}(x, \mathbf{k}) \right] \quad (2) \end{aligned}$$

where $x_+ = x + \omega$, $\mathbf{k}_+ = \mathbf{k} + \mathbf{q}$, $l_i = 1, \dots, 5$ represents the d -orbital, and A (R) represents the advanced (retarded) Green function. $\rho_{ll'}^{\text{G}}(x, \mathbf{k}) \equiv (G_{ll'}^{\text{A}}(x, \mathbf{k}) - G_{ll'}^{\text{R}}(x, \mathbf{k}))/2\pi i$ and $\rho_{ll'}^{\text{F}(\dagger)}(x, \mathbf{k}) \equiv (F_{ll'}^{\dagger \text{A}}(x, \mathbf{k}) - F_{ll'}^{\dagger \text{R}}(x, \mathbf{k}))/2\pi i$ are one particle spectral functions. Here, we divide $\hat{\chi}^{\text{OR(A)}}$ into the “Hermite part” $\hat{\chi}^{0'}$ and “non-Hermite part” $\hat{\chi}^{0''}$,

$$\begin{aligned} \hat{\chi}^{\text{OR(A)}} &\equiv \hat{\chi}^{0'} + (-)i\hat{\chi}^{0''} \\ &= \left[\frac{\hat{\chi}^{\text{OR}} + \hat{\chi}^{0\text{A}}}{2} \right] + (-)i \left[\frac{\hat{\chi}^{\text{OR}} - \hat{\chi}^{0\text{A}}}{2i} \right]. \end{aligned} \quad (3)$$

Then, $\hat{\chi}^{0'}$ and $\hat{\chi}^{0''}$ are expressed as

$$\begin{aligned} \hat{\chi}_{l_1 l_2, l_3 l_4}^{0'}(\omega, \mathbf{q}) &= \frac{\pi}{2N} \sum_{\mathbf{k}} \int dx \\ &\left[\tanh \frac{x}{2T} \Theta_{l_1 l_3}^{\text{G}}(x_+, \mathbf{k}_+) \rho_{l_4 l_2}^{\text{G}}(x, \mathbf{k}) \right. \\ &+ \tanh \frac{x_+}{2T} \rho_{l_1 l_3}^{\text{G}}(x_+, \mathbf{k}_+) \Theta_{l_4 l_2}^{\text{G}}(x, \mathbf{k}) \\ &+ \tanh \frac{x}{2T} \Theta_{l_1 l_4}^{\text{F}}(x_+, \mathbf{k}_+) \rho_{l_3 l_2}^{\text{F}\dagger}(x, \mathbf{k}) \\ &\left. + \tanh \frac{x_+}{2T} \rho_{l_1 l_4}^{\text{F}}(x_+, \mathbf{k}_+) \Theta_{l_3 l_2}^{\dagger \text{F}}(x, \mathbf{k}) \right] \quad (4) \end{aligned}$$

$$\begin{aligned} \hat{\chi}_{l_1 l_2, l_3 l_4}^{0''}(\omega, \mathbf{q}) &= \frac{\pi}{2N} \sum_{\mathbf{k}} \int dx \\ &\left[\tanh \frac{x_+}{2T} - \tanh \frac{x}{2T} \right] \\ &\times \left[\rho_{l_1 l_3}^G(x_+, \mathbf{k}_+) \rho_{l_4 l_2}^G(x, \mathbf{k}) \right. \\ &\left. + \rho_{l_1 l_4}^F(x_+, \mathbf{k}_+) \rho_{l_3 l_2}^{F\dagger}(x, \mathbf{k}) \right], \quad (5) \end{aligned}$$

where we denote $\Theta_{ll'}^G(x, \mathbf{k}) \equiv (G_{ll'}^A(x, \mathbf{k}) + G_{ll'}^R(x, \mathbf{k}))/2\pi$ and $\Theta_{ll'}^{F(\dagger)}(x, \mathbf{k}) \equiv (F_{ll'}^{(\dagger)A}(x, \mathbf{k}) + F_{ll'}^{(\dagger)R}(x, \mathbf{k}))/2\pi$.

We explain that the non-Hermite part satisfies the relation $\hat{\chi}^{0''}(\omega, \mathbf{q}) = 0$ for $|\omega| < 2\Delta$ at $T = 0$. Now, we assume $\omega > 0$. $\rho_{ll'}^{G,F}(x, \mathbf{k}) = 0$ is given for $|x| < \Delta$ since the SC gap opens. Then, in order to satisfy both $\rho_{ll'}^{G,F}(x, \mathbf{k}) \neq 0$ and $\rho_{ll'}^{G,F}(x_+, \mathbf{k}_+) \neq 0$, inequalities $|x_+| > \Delta$ and $|x| > \Delta$ are required. Moreover, $[\tanh \frac{x_+}{2T} - \tanh \frac{x}{2T}] \neq 0$ only when $x_+ \cdot x < 0$. In order to obtain the finite value of $\hat{\chi}^{0''}(\omega, \mathbf{q})$ in eq. (5), all three inequalities must be satisfied for some x . Considering the third inequality, the first two inequalities are restricted to

$$x_+ > \Delta, \quad (6)$$

$$x < -\Delta. \quad (7)$$

They are satisfied for some x only when $\omega > 2\Delta$. Therefore, $\hat{\chi}^{0''}(\omega, \mathbf{q}) \neq 0$ for $|\omega| > 2\Delta$, while $\hat{\chi}^{0''}(\omega, \mathbf{q}) = 0$ for $|\omega| < 2\Delta$.

In the present numerical study, we calculate exactly $\hat{\chi}^{0''}$ using eq. (5), and calculate approximately $\hat{\chi}^{0'}$ using the Hermite part of eq. (6) in Ref.⁴⁹. Using this method, we can calculate accurately the imaginary part of the spin susceptibility as we will discuss later.

Then, the spin susceptibility $\chi^s(\omega, \mathbf{q})$ is given by the multiorbital random-phase-approximation (RPA) with the intraorbital Coulomb U , interorbital Coulomb U' , Hund coupling J , and pair-hopping J'^{13} :

$$\chi^s(\omega, \mathbf{q}) = \sum_{i,j} \left[\frac{\hat{\chi}^{0R}(\omega, \mathbf{q})}{1 - \hat{S}^0 \hat{\chi}^{0R}(\omega, \mathbf{q})} \right]_{ii,jj}, \quad (8)$$

where vertex of spin channel $\hat{S}_{l_1 l_2, l_3 l_4}^0 = U, U', J$ and J' for $l_1 = l_2 = l_3 = l_4$, $l_1 = l_3 \neq l_2 = l_4$, $l_1 = l_2 \neq l_3 = l_4$ and $l_1 = l_4 \neq l_2 = l_3$, respectively. Hereafter, we put $J = J' = 0.15\text{eV}$, $U' = U - 2J$, and fix the electron number as 6.1 (10% electron-doped case). In the present model, $\chi^s(0, \mathbf{q})$ takes the maximum value when \mathbf{q} is the nesting vector $\mathbf{Q} = (\pi, \pi/8)$. Due to the nesting, $\chi^s(0, \mathbf{Q})/\chi^0(0, \mathbf{Q}) \approx 1/(1 - \alpha_{\text{St}})$ is enhanced; $\alpha_{\text{St}} (\lesssim 1)$ is the maximum eigenvalue of $\hat{S}^0 \hat{\chi}^{0R}(0, \mathbf{Q})$ that is called the Stoner factor.

In the following, we prove that the non-Hermite part of spin susceptibility $\text{Im}\chi^s(\omega, \mathbf{q}) \equiv [\chi^{\text{sR}}(\omega, \mathbf{q}) - \chi^{\text{sA}}(\omega, \mathbf{q})]/2i$ is zero for $|\omega| < 2\Delta$ at $T = 0$, except at the resonance energy ω_{res} for the s_{\pm} -wave state: The spin susceptibility is expressed as $\chi^{\text{sR(A)}}(\omega, \mathbf{q}) = \sum_{l,m} [\hat{\chi}^{\text{sR(A)}}]_{ll,mm}$, where $\hat{\chi}^{\text{sR(A)}}$ \equiv

$\hat{\chi}^{0R(A)}[1 - \hat{S}^0 \hat{\chi}^{0R(A)}]^{-1}$. As explained, $\hat{\chi}^{0''} = 0$ is satisfied for $\omega < 2\Delta$. Then, we obtain $\hat{\chi}^{\text{sR}} = \hat{\chi}^{\text{sA}} = \hat{\chi}^{0'}[1 - \hat{S}^0 \hat{\chi}^{0'}]^{-1}$. As a result $\hat{\chi}^{\text{sR}} - \hat{\chi}^{\text{sA}} = 0$ for $\omega < 2\Delta$ except when $\det[1 - \hat{S}^0 \hat{\chi}^{0'}] = 0$, which is satisfied at $\omega = \omega_{\text{res}}$ in the s_{\pm} -wave state. Thus, if we perform the numerical calculation of Eqs. (3)-(8) accurately, $\text{Im}\chi^s(\omega, \mathbf{Q}) = 0$ should be satisfied for $\omega < 2\Delta$.

B. Inelastic QP damping rate γ^*

In strongly correlated systems, $\chi^s(\omega, \mathbf{q})$ is renormalized by the self-energy correction. We phenomenologically introduce a band-diagonal self-energy as $z \cdot \text{Im}\hat{\Sigma}_{\mathbf{k}}^R(\epsilon) = i\gamma^*(\epsilon)\hat{1}$, where $z \equiv m/m^*$ is the renormalization factor. First, we estimate the QP damping in the normal state from the experimentally observed conductivity. From the Nakano-Kubo formula, the conductivity is given by $\sigma = e^2 \sum_{\nu} N_{\nu}(0) v_{\nu}^2 / 2\gamma(0)$, where $\gamma(0) \equiv \gamma^*(0)/z$ is the ‘‘unrenormalized’’ damping at zero energy, and $N_{\nu}(0)$ and v_{ν} are the density of states (DOS) and the Fermi velocity of the ν -th FS, respectively. Using the five-orbital model, we obtain $\rho \approx (2.0\gamma(0)[\text{meV}]) \mu\Omega\text{cm}$ for the inter-layer spacing $c = 6\text{\AA}$ and $\rho \approx (2.8\gamma(0)[\text{meV}]) \mu\Omega\text{cm}$ for $c = 8\text{\AA}$.^{26,27} In table I, we show the T -dependence of ρ estimated by fitting the experimental data below $\sim 100\text{K}$ ⁵²⁻⁵⁴, and the inelastic damping $\gamma(0)$ is derived from the theoretical relation between ρ and γ . For example, in $\text{BaFe}_{1.85}\text{Co}_{0.15}\text{As}_2$ ($c \approx 6\text{\AA}$), the unrenormalized inelastic damping $\gamma(0)$ is estimated as $3.7T$, which is comparable to that in over-doped cuprates.

Then, we derive the (ϵ, T) -dependences of the ‘‘renormalized’’ inelastic scattering: In the presence of the strong spin and orbital fluctuations, the damping follows the approximate relation $\gamma^*(\epsilon) \approx b(T + |\epsilon|/\pi)$ according to spin (orbital) fluctuation theories.^{12,55} According to Table I, we obtain $b \sim 1.9$ in $\text{BaFe}_{1.85}\text{Co}_{0.15}\text{As}_2$ if we assume $z \sim 0.5$. In the present study, we use a larger value $b = 2.5$. Note that the result is not so sensitive to the value of b .

In the present numerical study, we assume more simple ϵ -dependence of $\gamma^*(\epsilon)$ to simplify the analysis, justified in calculating $\text{Im}\chi^s$ for $0 \leq |\omega| \lesssim 4\Delta$. In the normal state, we put

$$\gamma^*(\epsilon) = \gamma_0^*. \quad (9)$$

In the SC state at $T \ll T_c$, $\gamma^*(\epsilon) = 0$ for $|\epsilon| < 3\Delta$ (= a particle-hole excitation gap (2Δ) plus a single-particle excitation gap (Δ)), while its functional form approaches to that of the normal state for $|\epsilon| \gtrsim 3\Delta$. Taking these facts into account, we put

$$\gamma^*(\epsilon) = a(\epsilon)\gamma_0^*, \quad (10)$$

where (i) $a(\epsilon) \ll 1$ for $|\epsilon| < 3\Delta$, (ii) $a(\epsilon) = 1$ for $|\epsilon| > 4\Delta$, and (iii) linear extrapolation for $3\Delta < |\epsilon| < 4\Delta$; see Fig. 1. We have confirmed that the obtained results are insensitive to the boundary of $|\epsilon|$ (4Δ in the present

	Ba _{1-x} K _x Fe ₂ As ₂ [$T_c = 37\text{K}$] ⁵²	BaFe _{1.85} Co _{0.15} As ₂ [$T_c = 25\text{K}$] ⁵³	LaFeAsO _{0.89} F _{0.11} [$T_c = 28\text{K}$] ⁵⁴
$\rho(T) - \rho(0)$ [$\mu\Omega\text{cm}$]	$\sim 23T$	$\sim 7.3T$	$\sim 4.6T^2$
$\gamma(0)$ [meV] at T	$\sim 12T$	$\sim 3.7T$	$\sim 1.6T^2$
$\gamma(0)$ [meV] at T_c	~ 37	~ 7.9	~ 9.3

TABLE I: $\rho(T) - \rho(0)$ and “unrenormalized” inelastic damping at zero energy $\gamma(0)$ ($= \gamma^*(0)/z$) estimated by fitting the experimental data below $\sim 100\text{K}$.^{52–54}. The unit of T is [meV].

case) between (ii) and (iii). Since $\gamma^*(\epsilon)$ is an increase function of T , γ_s^* at $T \ll T_c$ should be smaller than γ_0^* . Here, we derive the values of γ_s^* and γ_0^* from the relations $\gamma^*(\epsilon) \sim 2.5(T + |\epsilon|/\pi)$, by putting $\epsilon = 3\Delta = 15\text{meV}$ since we are interested in the hump structure around $\omega \sim 3\Delta$. Therefore, we put $\gamma_0^* = \gamma^*(3\Delta) = 20\text{meV}$ at $T = 3\text{meV}$ in the normal state. Similarly, we put $\gamma_s^* = \gamma^*(3\Delta) = 10\text{meV}$ at $T = 0$ in the superconducting state. In the $s_{++}(\pm)$ -wave state, we put $\Delta = 5\text{meV}$ for the two hole-pockets and $\Delta = (-)5\text{meV}$ for electron-pockets. In the numerical calculation, we use 3072×3072 \mathbf{k} -meshes and $a(\epsilon)\gamma_s^* = 0.5\text{meV}$ ($= 0.1\Delta$) for $|\epsilon| < 3\Delta$.

C. Hump structure in $\text{Im}\chi^s$ due to dissipationless QPs ($E_k < 3\Delta$)

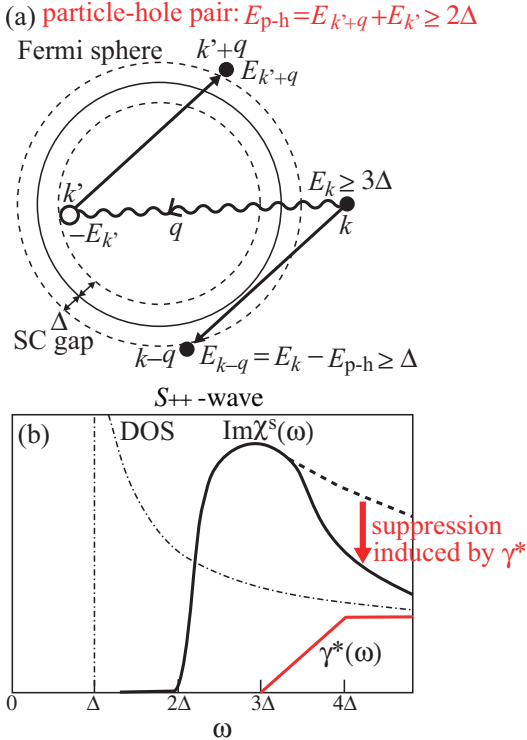


FIG. 1: (Color online) (a) Schematic inelastic scattering process in the SC state, by creating a particle-hole excitation 2Δ . The realization condition is $E_k \geq 3\Delta$. (b) Energy dependences of the DOS, $\gamma^*(\omega)$, and $\text{Im}\chi^s(\omega)$ in the s_{++} -wave state.

Here, we explain an intuitive reason why the QP is “dissipationless” for $|\omega| < 3\Delta$ at zero temperatures.³⁰ In Fig. 1 (a), we show an inelastic scattering process, in which a QP at \mathbf{k} is scattered to $\mathbf{k} - \mathbf{q}$, with exciting a particle-hole (p-h) pair ($\mathbf{k}' + \mathbf{q}, \mathbf{k}'$). Since a QP in the SC state cannot exist in the thin shell $|\omega| < \Delta$, the particle-hole excitation energy E_{p-h} is always larger than 2Δ . Since the energy of the final state $E_{\mathbf{k}-\mathbf{q}}$ is also larger than Δ , the inelastic scattering is prohibited when $E_{\mathbf{k}} \leq 3\Delta$. Thus, the relationship $\gamma^*(\omega) = 0$ for $|\omega| < 3\Delta$ is obtained. From this relation, the peak of the DOS at $\omega = \Delta$ for the isotropic SC gap remains to be sharp.

Then, the dissipationless QPs in the SC state produce the hump-shaped enhancement in the spin spectrum. In the normal state, $\text{Im}\chi^s$ has no gap structure, and it is suppressed by the inelastic QP damping γ^* induced by the strong correlation. In the SC state as illustrated in Fig. 1 (b), $\text{Im}\chi^s$ has the p-h excitation gap 2Δ . Since the QP is dissipationless for $|\omega| < 3\Delta$ in the SC state, the suppression in $\text{Im}\chi^s(\omega)$ is released just above the excitation gap $\omega \gtrsim 2\Delta$ so as to form a hump structure. For this reason, a prominent hump structure appears in $\text{Im}\chi^s(\omega, \mathbf{Q})$ just above 2Δ till $\sim 3\Delta$ in strongly correlated s_{++} -wave superconductors.

III. NUMERICAL RESULT

A. Spin susceptibility at the nesting vector $\mathbf{Q} = (\pi, \pi/8)$

Figure 2 shows the obtained $\text{Im}\chi^s(\omega, \mathbf{Q})$ at the nesting vector between the hole- and electron-pockets $\mathbf{Q} = (\pi, \pi/8)$: We fix $T = 1\text{meV}$ hereafter, since the obtained results are insensitive to the temperature for $T \leq 3\text{meV}$. In the normal state with $\gamma_0^* = 20(15)\text{meV}$, the Stoner factor is $\alpha_{\text{St}} = 0.950(0.959)$ for $U = 1.32\text{eV}$. In the SC states with $\gamma_s^* = 10\text{meV}$, $\alpha_{\text{St}} = 0.956(0.982)$ in the s_{++} -wave (s_{\pm} -wave) state for $U = 1.32\text{eV}$. In the s_{\pm} -wave state, α_{St} increases due to the coherence factor. Inversely, α_{St} in the s_{++} -wave state decreases due to absence of coherence factor. As shown in Fig. 2, in the normal state with $\gamma_0^* = 20\text{meV}$, the peak position of $\text{Im}\chi^s$ is about $20 - 25\text{meV}$, which is consistent with experimental result in BaFe_{1.85}Co_{0.15}As₂⁴⁰. Thus, the value of $\text{Im}\chi^s$ in the normal state with $\gamma_0^* = 15\text{meV}$ is overestimated.

A broad hump structure appears in the s_{++} -wave state at $\omega \gtrsim 2\Delta$ even in the case of $\Delta = 5\text{meV}$, and its

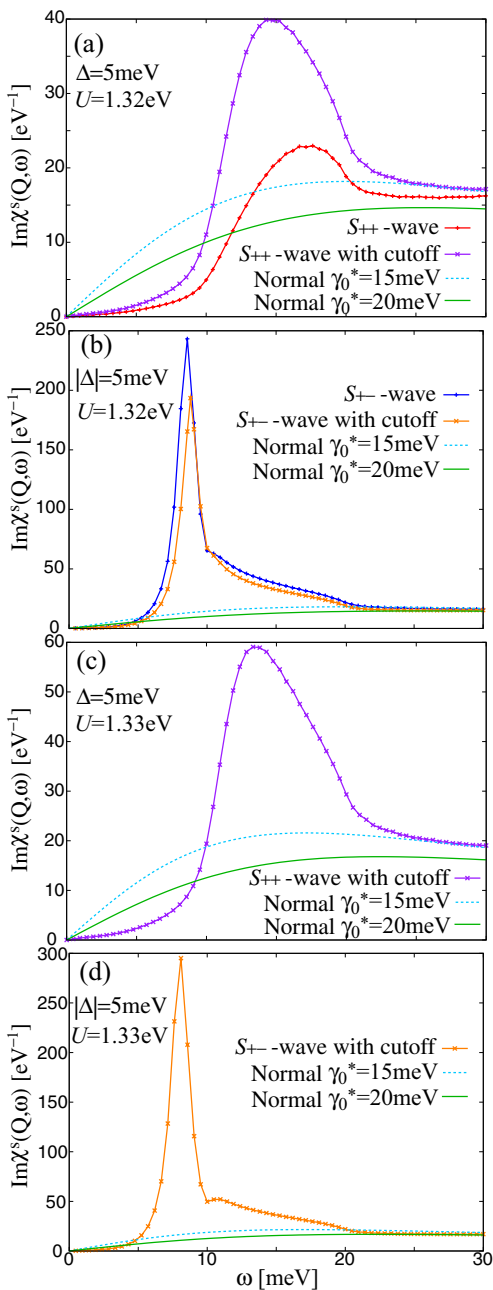


FIG. 2: (Color online) (a) ω -dependence of $\text{Im}\chi^s(\omega, \mathbf{Q})$ at $\mathbf{Q} = (\pi, \pi/8)$ for $U = 1.32\text{eV}$ in the s_{++} -wave state ($\Delta = 5\text{meV}$), as well as in the normal state with $\gamma_0^* = 15, 20\text{meV}$. The hump structure is enhanced by considering the high-energy dependence of the SC gap, by introducing the cut-off energy $\Delta E = 20\text{meV}$, (b) those in the s_{\pm} -wave state ($|\Delta| = 5\text{meV}$), (c) those for $U = 1.33\text{eV}$ in the s_{++} -wave state, and (d) those in the s_{\pm} -wave state.

overall shape is consistent with experimental results^{39,40}. We had neglected the energy-dependence of Δ in the previous study⁴⁹. However, in reality, the SC gap Δ will be cut off when the energy of the ν -th band $\epsilon_{\mathbf{k}}^{\nu}$ measured from the Fermi energy exceeds the characteristic energy scale of the pairing interaction. To take

this fact into account, we introduce a Gaussian cutoff $\Delta_{\mathbf{k}}^{\nu} = \Delta^{\nu} \exp\{-[\epsilon_{\mathbf{k}}^{\nu}/\Delta E]^2\}$ following Refs.^{50,56}. We put $\Delta E = 20\text{meV}$, which correspond to the Fe ion optical phonon frequency $\omega_{\text{D}} \sim 20\text{meV}$ employed in the orbital fluctuation theory.^{12,15}.

When the cutoff is applied in the s_{++} -wave state, the hump structure becomes more prominent as shown in Fig. 2 (a). We confirm that the obvious hump appears over the normal state even with $\gamma_0^* = 15\text{meV}$. The enhancement of hump structure originates from the increment of the Stoner factor by introducing the cutoff, from $\alpha_{\text{St}} = 0.956$ to 0.965 for $U = 1.32\text{eV}$.

On the other hand, in the s_{\pm} -wave state, very high and sharp resonance peak appears at $\omega_{\text{res}} < 2\Delta$ even in the case of $|\Delta| = 5\text{meV}$ as shown in Fig. 2 (b). This result is apparently inconsistent with experimental results. In order to explain the experimental result by the s_{\pm} -wave state, large inhomogeneity would be required, although the s_{\pm} -wave state is fragile against inhomogeneity. The height of the resonance peak exceeds 100eV^{-1} for $a(0)\gamma_s^* = 0.5\text{meV}$, while it diverges for $a(0) \rightarrow 0$ if \mathbf{k} -meshes are fine enough. $\text{Im}\chi^s$ is slightly suppressed by considering the cut off, $\Delta E = 20\text{meV}$.

We also study the spectra for both s_{++} - and s_{\pm} -wave states with cutoff for $U = 1.33\text{eV}$: In Fig. 2(c) and 2(d), we show the results for the normal state with $\gamma_0^* = 15\text{meV}$ ($\alpha_{\text{St}} = 0.965$) and $\gamma_0^* = 20\text{meV}$ ($\alpha_{\text{St}} = 0.956$). We also show results for the s_{++} -wave state with $\gamma_s^* = 10\text{meV}$ ($\alpha_{\text{St}} = 0.971$), and s_{\pm} -wave state with $\gamma_s^* = 10\text{meV}$ ($\alpha_{\text{St}} = 0.984$).

We note that the effect of multiband on $\text{Im}\chi^s$, which was discussed in Ref.⁴⁰, is automatically included in our calculation. By increasing U from 1.32eV to 1.33eV , the hump structure in the s_{++} -wave state is more enhanced. Also, the resonance peak in the s_{\pm} -wave state develops, and ω_{res} shifts to lower energy.

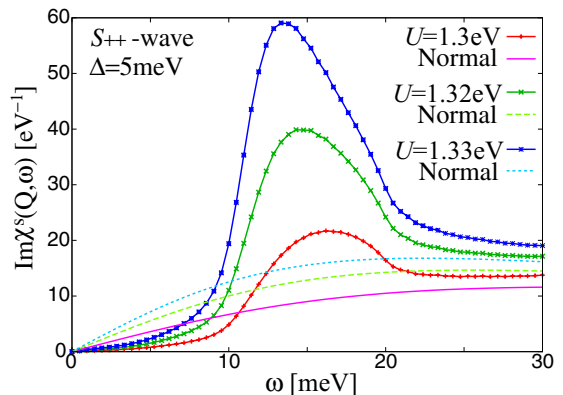


FIG. 3: (Color online) ω -dependence of $\text{Im}\chi^s(\omega, \mathbf{Q})$ at $\mathbf{Q} = (\pi, \pi/8)$ for $U = 1.3, 1.32,$ and 1.33eV in the s_{++} -wave state with $\Delta = 5\text{meV}$, and the cutoff energy $\Delta E = 20\text{meV}$, as well as normal states with $\gamma_0^* = 20\text{meV}$ for each value of U .

In Figure 3, we confirm that the hump in the s_{++} -wave with $\Delta = 5\text{meV}$ state is enhanced as the value of U

increases. Thus, the hump becomes prominent as system comes close to the AF order.

In this paper, we have calculated χ^s introduced in Eq. 8. To obtain the value of spin susceptibility χ^{neu} observed in neutron measurements, we have to take the spin magnetic moment ($= 1\mu_B$) and the factor of spin degeneracy. Its z -component is $\chi_z^{\text{neu}} = 2\chi^s[\mu_B^2\text{eV}^{-1}]$ and the transverse spin susceptibility is $\chi_{\pm}^{\text{neu}} = 4\chi^s[\mu_B^2\text{eV}^{-1}]$.

B. Comparison with our previous method

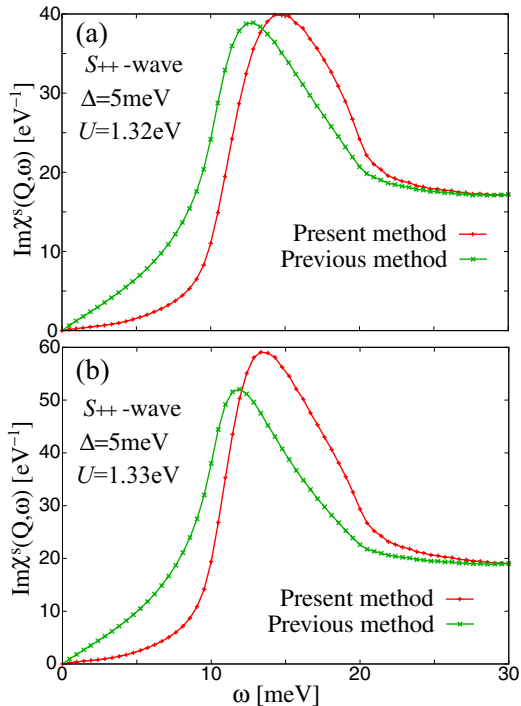


FIG. 4: (Color online) $\text{Im}\chi^s(\omega, \mathbf{Q})$ at $\mathbf{Q} = (\pi, \pi/8)$ for $U = 1.32\text{eV}$ (a) and $U = 1.33\text{eV}$ (b) in the s_{++} -wave state ($\Delta = 5\text{meV}$). We show the comparison between the present improved method and the previous method in Ref.⁴⁹, with the cutoff ($\Delta E = 20\text{meV}$).

In the s_{++} -wave state, $\text{Im}\chi^s(\omega, \mathbf{Q}) = 0$ for $|\omega| < 2\Delta$ at $T = 0$ as we discussed in Sec. II. This relation is correctly satisfied in the present method if we put $a(0) \rightarrow 0$ in Eq. (10). In the present method, we perform the numerical calculation of $\hat{\chi}^{0''}$ using Eq. (5) exactly. In fact, in Fig. 4(a) and (b), we verify that the spectral gap of $\text{Im}\chi^s(\omega, \mathbf{Q})$ is well reproduced in the present method with $a(0)\gamma_s^* = 0.5\text{meV}$, demonstrating the superiority of the present method to the previous method in Ref.⁴⁹. In the case of s_{\pm} -wave state, we obtain $\text{Im}\chi^s(\omega, \mathbf{Q}) \propto \delta(\omega - \omega_{\text{res}})$ for $|\omega| < 2\Delta$ if the numerical calculation is performed accurately.

In the present paper, we calculate $\hat{\chi}^{0''}$ in eq. (5) exactly, while $\hat{\chi}^{0'}$ is calculated approximately using eqs. (6) and (7) in Ref.⁴⁹. We consider this is justified since we

had verified that the present ‘‘approximated RPA’’ is reliable in our previous paper⁴⁹: In Fig. 1 (b) of Ref.⁴⁹, we had performed the ‘‘exact RPA calculation’’ for both $\hat{\chi}^{0'}$ and $\hat{\chi}^{0''}$ with $\Delta = 400\text{meV}$, and confirmed that overall behavior of $\text{Im}\chi^s(\omega, \mathbf{Q})$ is well reproduced by the present approximated RPA.

Here, we comment on the \mathbf{q} dependence of $\text{Im}\chi^s(\omega, \mathbf{q})$ around $\mathbf{q} = \mathbf{Q}$. In our two-dimensional model¹³, it is difficult to discuss the \mathbf{q} dependence of $\text{Im}\chi^s(\omega, \mathbf{q})$ because \mathbf{q} dependence of $\text{Im}\chi^s(\omega, \mathbf{q})$ is drastic even in the normal state, which is inconsistent with the neutron scattering measurements.

C. Comparison with Nagai *et al.*⁵⁰

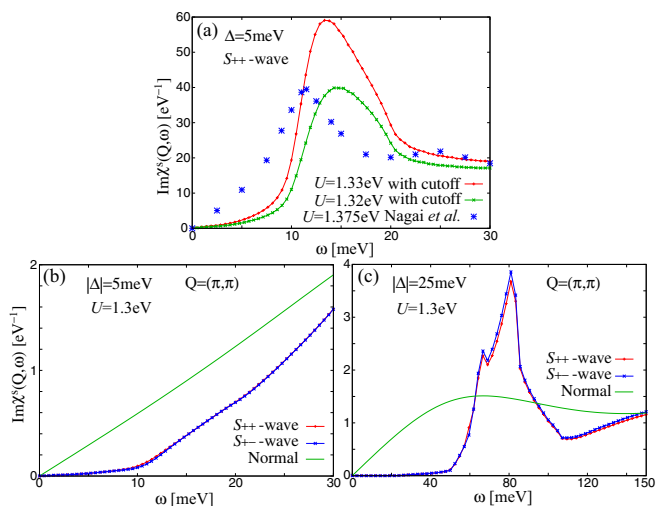


FIG. 5: (Color online) (a) $\text{Im}\chi^s(\omega, \mathbf{q})$ in the s_{++} -wave state ($\Delta = 5\text{meV}$) for $U = 1.32\text{eV}$ and 1.33eV obtained in the present study. We also plot the data of Nagai *et al.*⁵⁰ for $U = 1.375\text{eV}$, by multiplying 0.39. All results are obtained for the cutoff energy $\Delta E = 20\text{meV}$. (b) $\text{Im}\chi^s(\omega, \mathbf{q})$ at $\mathbf{q} = (\pi, \pi)$ for $U = 1.3\text{eV}$ in both s_{++} - and s_{\pm} -wave states with $|\Delta| = 5\text{meV}$ and $\gamma_s^* = 10\text{meV}$, together with the result in the normal state for $\gamma_0^* = 20\text{meV}$. (c) $\text{Im}\chi^s(\omega, \mathbf{q})$ at $\mathbf{q} = (\pi, \pi)$ in both s_{++} - and s_{\pm} -wave states with $|\Delta| = 25\text{meV}$ and $\gamma_s^* = 50\text{meV}$, together with the result in the normal state for $\gamma_0^* = 50\text{meV}$.

Recently, Nagai *et al.*⁵⁰ had calculated the neutron scattering spectrum using the method proposed in Ref.⁴⁹, and claimed that (i) hump structure in the s_{++} -wave state is smeared when $\gamma^* \sim 10\text{meV}$ and $\Delta \sim 5\text{meV}$ compared to the case of $\Delta > 25\text{meV}$, and (ii) resonance peak in the s_{\pm} -wave state becomes very low and broad. Moreover, they had also claimed that (iii) one can distinguish between the s_{++} -wave and the s_{+-} -wave states from the spectrum at $\mathbf{q} = (\pi, \pi)$.

First, we explain that (i) and (ii) are incorrect statements based on their inaccurate numerical calculation. First, their result fails to reproduce the spectral gap of $\text{Im}\chi^s$ for $\omega < 2\Delta$ as shown in Fig. 5 (a). (One can prove

rigorously that $\text{Im}\chi^s = 0$ for $\omega < 2\Delta$ at $T = 0$.) Second, the peak position of the result of Nagai *et al.*⁵⁰ is about 2Δ , while it must be higher energy ($\sim 3\Delta$). In the s_{\pm} -wave state, the resonance peak should be δ functional structure when $a(0)$ in eq. (10) is enough smaller than Δ . Thus, the low and broad resonance peak of Nagai *et al.*⁵⁰ is far from the exact behavior of the resonance peak. In Nagai's results, fine structures in $\text{Im}\chi^s(\omega, \mathbf{q})$ seem to be inappropriately smeared in both s_{++} - and s_{\pm} -wave states.

Next, we comment on the claim (iii). They pointed out the spectrum in the s_{\pm} -wave state with $\Delta = 5\text{meV}$ are different from that in the s_{++} -wave state with $\Delta = 25\text{meV}$. Here, we show the results of both s_{++} - and s_{\pm} -wave states in Figs. 5, for (b) $|\Delta| = 5\text{meV}$ and (c) $|\Delta| = 25\text{meV}$. Since both spectra are almost identical, we cannot distinguish between the s_{++} - and s_{\pm} -wave states by the spectrum at the wave vector $\mathbf{q} = (\pi, \pi)$ for the same Δ . This result is reasonable because sign of the SC gap is preserved through the (π, π) shift for both the s_{++} - and s_{\pm} -wave states. Although claim (iii) is based on their numerical result in which the hump of the s_{++} -wave state appears only for $\Delta \gtrsim 25\text{meV}$, the prominent hump appears in the s_{++} -wave state with $\Delta = 5\text{meV}$ in our improved numerical results as shown in Fig. 2(a) and (c). Thus, we conclude it is impossible to distinguish between the s_{++} - and s_{\pm} -wave states with $\Delta = 5\text{meV}$.

IV. CONCLUSION

We have studied the dynamical spin susceptibility $\chi^s(\omega, \mathbf{Q})$ in iron-based superconductors for both s_{++} - and s_{\pm} -wave states, by developing more accurate numerical method and introducing the high-energy dependence of the SC gap.⁴⁹ In the s_{++} -wave state, the dissipationless QPs for $|\omega| < 3\Delta$ produce a prominent hump-shaped enhancement in $\chi^s(\omega, \mathbf{Q})$ just above 2Δ till $\sim 3\Delta$. This ‘‘dissipationless mechanism’’ is unrelated to the resonance. The peak energy of the hump will shift to lower energy if we consider the band-dependence and/or the anisotropy of the SC gap, as we discussed in Ref.⁴⁹.

On the other hand, in the s_{\pm} -wave state, very high and sharp resonance peak appears at $\omega_{\text{res}} < 2\Delta$. In order to explain small and broad peaks observed in Refs.^{39,40} as the resonance peak in the s_{\pm} -wave state, sufficient inhomogeneity or small SC volume fraction would be required. However, the s_{\pm} -wave state is fragile against inhomogeneity. We concluded that the small and broad spectral peak observed in iron pnictides is naturally reproduced based on the s_{++} -wave state in the absence of inhomogeneity, rather than the s_{\pm} -wave state.

In the Comment on the present paper written by Nagai and Kuroki on arXiv⁵⁷, the authors repeated their claim ‘‘smallness of the hump in the s_{++} -wave state’’ based on the ‘‘old method’’ that was first developed in Ref.⁴⁹. In Sec. III, however, we actually obtained large hump using the ‘‘new method’’, which is mathematically superior to

the old method. This discrepancy originates from the calculation method as well as the numerical accuracy, not from the detail of model parameters, as we discussed in our Reply on arXiv⁵⁸.

Acknowledgments

We are grateful to M. Sato, Y. Kobayashi, Y. Matsuda, D. S. Hirashima, D. J. Scalapino, P. J. Hirschfeld, A. V. Chubukov, I. Eremin, Y. Tanaka and K. Kuroki, for valuable discussions. This study has been supported by Grants-in-Aid for Scientific Research from MEXT of Japan, and by JST, TRIP. Numerical calculations were performed at the Computer Center and the ISSP Supercomputer Center of University of Tokyo, and the Yukawa Institute Computer Facility.

Appendix A: Hump structure in the neutron inelastic scattering for a Kondo semiconductor CeNiSn

In this paper, we have studied the neutron inelastic scattering spectrum in iron pnictide superconductors. In the s_{++} -wave SC state, we confirmed that a large hump structure appears just above 2Δ due to the reduction in the inelastic QP scattering γ^* , which is the most important finding in this paper.

Then, a natural question is whether such a hump-shaped enhancement by ‘‘dissipationless mechanism’’ is universal or not. To answer this question, we discuss a Kondo semiconductor CeNiSn. Figure 6 (a) shows the neutron inelastic scattering spectrum in CeNiSn at $\mathbf{q} = (0, \pi, 0)$ at low temperatures⁵⁹. The observed large and broad hump structure in CeNiSn^{59,60} is very similar to that in iron pnictides. CeNiSn is an incoherent metal with large inelastic scattering above the Kondo temperature $T_K \sim 30\text{K}$, while it becomes a semiconductor with c - f hybridization gap in the single-particle spectrum (Δ) much below T_K .

The effective model for the CeNiSn is described as the periodic Anderson model (PAM) at half-filling.^{61–63} Neglecting the f -orbital degeneracy, the PAM is given as

$$\mathcal{H} = \sum_{\mathbf{k}, \sigma} \epsilon_c^c c_{\mathbf{k}\sigma}^\dagger c_{\mathbf{k}\sigma} + \epsilon_f \sum_{\mathbf{k}, \sigma} f_{\mathbf{k}\sigma}^\dagger f_{\mathbf{k}\sigma} + U \sum_i f_{i\uparrow}^\dagger f_{i\uparrow} f_{i\downarrow}^\dagger f_{i\downarrow} + V \sum_{\mathbf{k}, \sigma} \left(f_{\mathbf{k}\sigma}^\dagger c_{\mathbf{k}\sigma} + c_{\mathbf{k}\sigma}^\dagger f_{\mathbf{k}\sigma} \right), \quad (\text{A1})$$

where $c_{\mathbf{k}\sigma}$ ($c_{\mathbf{k}\sigma}^\dagger$) and $f_{\mathbf{k}\sigma}$ ($f_{\mathbf{k}\sigma}^\dagger$) are annihilation (creation) operators for c - and f -electrons, respectively. V is the c - f mixing potential, and U is the Coulomb interaction for f -electrons. Here, the bandwidth is 2. Mutou and Hirashima studied this model at half-filling using the dynamical mean-field theory (DMFT) and the quantum Monte Carlo (QMC)⁶². Hereafter, we introduce their numerical results and discuss the energy-dependence of

$\text{Im}\chi^s(\omega)$. Readers can find more detailed explanations in the original paper⁶².

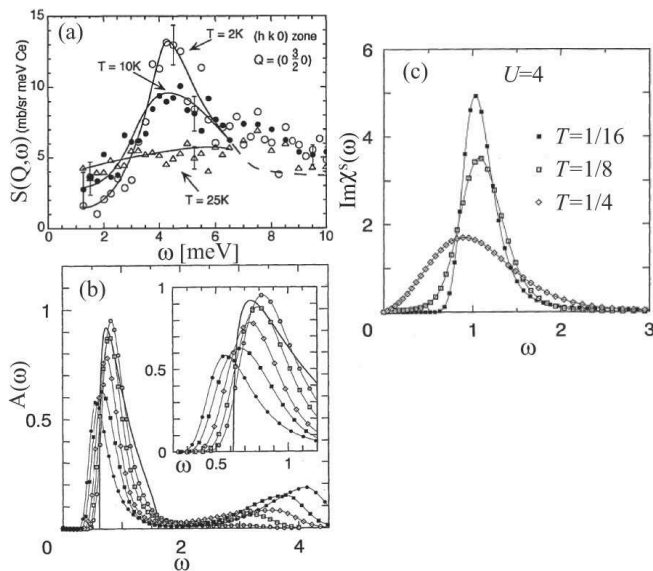


FIG. 6: (a) ω -dependence of $S(\mathbf{Q}, \omega) = \text{Im}\chi^s/(1 - e^{-\omega/T})$ in CeNiSn at various temperatures⁵⁹. (b) Single-particle spectrum $A(\omega)$ at $T = 1/16$ for $U = 0$ (solid curve), 1 (open circles), 2 (open squares), 3 (open diamonds), 4 (solid squares) and 5 (solid circles)⁶². The inset shows the low frequency part. (c) $\text{Im}\chi^s(\omega)$ for $U = 4$ at different temperatures⁶².

Figure 6 (b) shows the obtained single-particle spectrum $A(\omega)$. For $U = 0$, the hybridization gap in $A(\omega)$ is $\Delta = 0.62$. For $U = 4$, Δ is renormalized to 0.35 at $T = 1/16$ ($\ll T_K$), while the gap is smeared out by thermal fluctuations above T_K ⁶². At $T = 0$, inelastic QP scattering is suppressed by the hybridization gap, such that $\gamma^*(\omega) = 0$ for $|\omega| < 3\Delta$ ⁶³ in analogy to Fig. 1 (a).

Figure 6 (c) shows $\text{Im}\chi^s(\omega)$ for $U = 4$. In the metallic state at $T = 1/4$ ($\gg T_K$), $\text{Im}\chi^s(\omega)$ shows a gapless metallic behavior. In the semiconducting state at $T = 1/16$ ($\ll T_K$), in contrast, it shows a spectral gap Δ_s and the relation $\Delta_s \approx 2\Delta \approx 0.7$ is recognized. At the same time, large hump structure emerges around $\omega \sim 3\Delta$. Because of the absence of spin resonance mechanism, its natural explanation is the reduction in the inelastic QP scattering ($\gamma^*(\omega) = 0$ for $|\omega| < 3\Delta$), as we discussed in Fig. 1 (b). We must stress the hump structure in Fig. 6 (c) is obtained *exactly in the DMFT*, by including both the self-energy and vertex corrections. Therefore, experimental and theoretical studies in CeNiSn strongly support the idea of “hump structure in the s_{++} -wave state” given in Fig. 2 (a), that is obtained by the RPA by introducing the inelastic QP scattering $\gamma^*(\omega)$ phenomenologically.

¹ Y. Kamihara, T. Watanabe, M. Hirano, and H. Hosono, J. Am. Chem. Soc. **130**, 3296 (2008).
² K. Hashimoto, T. Shibauchi, T. Kato, K. Ikada, R. Okazaki, H. Shishido, M. Ishikado, H. Kito, A. Iyo, H. Eisaki, S. Shamoto, and Y. Matsuda, Phys. Rev. Lett. **102**, 017002 (2009).
³ D. V. Evtushinsky, D. S. Inosov, V. B. Zabolotnyy, M. S. Viazovska, R. Khasanov, A. Amato, H. -H. Klauss, H. Luetkens, C. Niedermayer, G. L. Sun, V. Hinkov, C. T. Lin, A. Varykhalov, A. Koitzsch, M. Knupfer, B. Buchner, A. A. Kordyuk, and S. V. Borisenko, New J. Phys. **11**, 055069 (2009).
⁴ K. Nakayama, T. Sato, P. Richard, Y. -M. Xu, Y. Sekiba, S. Souma, G. F. Chen, J. L. Luo, N. L. Wang, H. Ding, and T. Takahashi, Europhys. Lett. **85**, 67002 (2009).
⁵ Y. Kobayashi, A. Kawabata, S. C. Lee, T. Moyoshi, and M. Sato, J. Phys. Soc. Jpn. **78** (2009) 073704.
⁶ H. Mukuda, N. Terasaki, H. Kinouchi, M. Yashima, Y. Kitaoka, S. Suzuki, S. Miyasaka, S. Tajima, K. Miyazawa, P. Shirage, H. Kito, H. Eisaki, and A. Iyo, J. Phys. Soc. Jpn. **77**, 093704 (2008).
⁷ G. Fuchs, S. -L. Drechsler, N. Kozlova, M. Bartkowiak, G. Behr, K. Nenkov, H.-H. Klauss, J. Freudenberger, M. Knupfer, F. Hammerath, G. Lang, H. -J. Grafe, B. Buechner, and L. Schultz, Physica C **470**, S288 (2010).
⁸ K. Hashimoto, M. Yamashita, S. Kasahara, Y. Senshu, N. Nakata, S. Tonegawa, K. Ikada, A. Serafin, A. Carrington, T. Terashima, H. Ikeda, T. Shibauchi, and Y. Matsuda, Phys. Rev. B **81**, 220501(R) (2010).

⁹ Y. Kamihara, H. Hiramatsu, M. Hirano, R. Kawamura, H. Yanagi, T. Kamiya, and H. Hosono, J. Am. Chem. Soc. **128**, 10012 (2006).
¹⁰ C. W. Hicks, T. M. Lippman, M. E. Huber, J. G. Analytis, J. -H. Chu, A. S. Erickson, I. R. Fisher, and K. A. Moler, Phys. Rev. Lett. **103**, 127003 (2009).
¹¹ S. Graser, T. A. Maier, P. J. Hirschfeld, and D. J. Scalapino, New J. Phys. **11**, 025016 (2009).
¹² S. Onari and H. Kontani, arXiv:1009.3882.
¹³ K. Kuroki, S. Onari, R. Arita, H. Usui, Y. Tanaka, H. Kontani, H. Aoki, Phys. Rev. Lett. **101**, 087004 (2008); K. Kuroki, H. Usui, S. Onari, R. Arita, H. Aoki, Phys. Rev. B **79**, 224511 (2009).
¹⁴ I. I. Mazin, D. J. Singh, M. D. Johannes, and M. H. Du, Phys. Rev. Lett. **101**, 057003 (2008).
¹⁵ H. Kontani and S. Onari, Phys. Rev. Lett. **104**, 157001 (2010).
¹⁶ T. Saito, S. Onari, and H. Kontani, Phys. Rev. B **82**, 144510 (2010).
¹⁷ C. H. Lee, A. Iyo, H. Eisaki, H. Kito, M. T. Fernandez-Diaz, T. Ito, K. Kihou, H. Matsuhata, M. Braden, and K. Yamada, J. Phys. Soc. Jpn. **77**, 083704 (2008).
¹⁸ T. Shimojima, F. Sakaguchi, K. Ishizaka, Y. Ishida, T. Kiss, M. Okawa, T. Togashi, C.-T. Chen, S. Watanabe, M. Arita, K. Shimada, H. Namatame, M. Taniguchi, K. Ohgushi, S. Kasahara, T. Terashima, T. Shibauchi, Y. Matsuda, A. Chainani, and S. Shin, Science **332**, 564 (2011).
¹⁹ H. Kontani, T. Saito, and S. Onari, Phys. Rev. B **84**, 024528 (2011).

- ²⁰ T. Saito, S. Onari and H. Kontani, Phys. Rev. B **83**, 140512 (2011).
- ²¹ D. V. Efremov, M. M. Korshunov, O. V. Dolgov, A. A. Golubov, P. J. Hirschfeld, arXiv:1104.3840.
- ²² A. Kawabata, S.C. Lee, T. Moyoshi, Y. Kobayashi, and M. Sato, J. Phys. Soc. Jpn. **77**, 103704 (2008); S. C. Lee *et al.*, J. Phys. Soc. Jpn. **78**, 043703 (2009); M. Sato, Y. Kobayashi, S. C. Lee, H. Takahashi, E. Satomi, and Y. Miura, J. Phys. Soc. Jpn. **79**, 014710 (2010); T. Kawamata, E. Satomi, Y. Kobayashi, M. Itoh and M. Sato, J. Phys. Soc. Jpn. **80**, 084720 (2011).
- ²³ A. S. Sefat, R. Jin, M. A. McGuire, B. C. Sales, D. J. Singh, and D. Mandrus, Phys. Rev. Lett. **101**, 117004 (2008); A. Leithe-Jasper, W. Schnelle, C. Geibel, and H. Rosner, Phys. Rev. Lett. **101**, 207004 (2008).
- ²⁴ W. Schnelle, A. Leithe-Jasper, R. Gumeniuk, U. Burkhardt, D. Kasinathan, and H. Rosner, Phys. Rev. B **79**, 214516 (2009).
- ²⁵ L. Fang, H. Luo, P. Cheng, Z. Wang, Y. Jia, G. Mu, B. Shen, I. I. Mazin, L. Shan, C. Ren, H. -H. Wen, Phys. Rev. B **80**, 140508(R) (2009).
- ²⁶ S. Onari and H. Kontani, Phys. Rev. Lett. **103** (2009) 177001.
- ²⁷ H. Kontani and M. Sato, arXiv:1005.0942: The s_{++} -wave (d -wave) state disappears when the dimensionless scattering rate $g \equiv \gamma_{\text{imp}}^*/2\pi T_{c0}$ exceeds 0.23 (0.14). Since $g \propto \gamma_{\text{imp}}^*/T_{c0} \propto z\rho(0)/T_{c0}$, the SC state in heavy fermion superconductors with $z \sim 0.01$ survives till $\rho(0) \lesssim 50 \mu\Omega\text{cm}$ although their T_c 's are low.
- ²⁸ P. Monthoux and D. J. Scalapino, Phys. Rev. Lett. **72**, 1874 (1994)
- ²⁹ D. K. Morr and D. Pines, Phys. Rev. Lett. **81**, 1086 (1998).
- ³⁰ A. Abanov and A. V. Chubukov, Phys. Rev. Lett. **83**, 1652 (1999).
- ³¹ T. Takimoto and T. Moriya, J. Phys. Soc. Jpn. **67**, 3570 (1998).
- ³² S. Iikubo, M. Ito, A. Kobayashi, M. Sato and K. Kakurai, J. Phys. Soc. Jpn. **74**, 275 (2005).
- ³³ M. Ito, H. Harashina, Y. Yasui, M. Kanada, S. Iikubo, M. Sato, A Kobayashi, and K. Kakurai, J. Phys. Soc. Jpn. **71**, 265 (2002).
- ³⁴ H. F. Fong, P. Bourges, Y. Sidis, L. P. Regnault, A. Ivanov, G. D. Gu, N. Koshizuka, B. Keimer, Nature **398**, 588 (1999).
- ³⁵ C. Stock, C. Broholm, J. Hudis, H. J. Kang, and C. Petrovic, Phys. Rev. Lett. **100**, 087001 (2008).
- ³⁶ N. K. Sato, N. Aso, K. Miyake, R. Shiina, P. Thalmeier, G. Varelogiannis, C. Geibel, F. Steglich, P. Fulde, T. Komatsubara, Nature **410**, 340 (2001).
- ³⁷ T. A. Maier, S. Graser, P. J. Hirschfeld, and D. J. Scalapino, Phys. Rev. B **83**, 220505(R) (2011).
- ³⁸ A. D. Christianson, E. A. Goremychkin, R. Osborn, S. Rosenkranz, M. D. Lumsden, C. D. Malliakas, I. S. Todorov, H. Claus, D. Y. Chung, M. G. Kanatzidis, R. I. Bewley, and T. Guidi, Nature **456**, 930 (2008).
- ³⁹ Y. Qiu, W. Bao, Y. Zhao, C. Broholm, V. Stanev, Z. Tesanovic, Y. C. Gasparovic, S. Chang, J. Hu, B. Qian, M. Fang, and Z. Mao, Phys. Rev. Lett. **103**, 067008 (2009).
- ⁴⁰ D. S. Inosov, J. T. Park, P. Bourges, D. L. Sun, Y. Sidis, A. Schneidewind, K. Hradil, D. Haug, C. T. Lin, B. Keimer, and V. Hinkov, Nature Physics **6**, 178 (2010)
- ⁴¹ J. Zhao, L. -P. Regnault, C. Zhang, M. Wang, Z. Li, F. Zhou, Z. Zhao, C. Fang, J. Hu, P. Dai, Phys. Rev. B **81**, 180505 (2010).
- ⁴² S. Tatematsu, Y. Yasui, T. Moyoshi, K. Motoya, K. Kakurai, and M. Sato, to be published in J. Phys. Soc. Jpn.
- ⁴³ M. Sato *et al.*, unpublished.
- ⁴⁴ T. A. Maier and D. J. Scalapino, Phys. Rev. B **78**, 020514(R) (2008); T. A. Maier, S. Graser, D. J. Scalapino, and P. J. Hirschfeld, Phys. Rev. B **79**, 224510 (2009).
- ⁴⁵ M. M. Korshunov and I. Eremin, Phys. Rev. B **78**, 140509(R) (2008).
- ⁴⁶ K. Terashima, Y. Sekiba, J. H. Bowen, K. Nakayama, T. Kawahara, T. Sato, P. Richard, Y.-M. Xu, L. J. Li, G. H. Cao, Z. -A. Xu, H. Ding, and T. Takahashi, Proc. Natl. Acad. Sci. USA **106**, 7330 (2009).
- ⁴⁷ F. Hardy, P. Burger, T. Wolf, R. A. Fisher, P. Schweiss, P. Aadelmann, R. Heid, R. Fromknecht, R. Eder, D. Ernst, H. v. Lohneyzen, and C. Meingast, Europhys. Lett. **91**, 47008 (2010).
- ⁴⁸ L. Luan, T. M. Lippman, C. W. Hicks, J. A. Bert, O. M. Auslaender, J. -H. Chu, J. G. Analytis, I. R. Fisher, and K. A. Moler, Phys. Rev. Lett. **106**, 067001 (2011).
- ⁴⁹ S. Onari, H. Kontani and M. Sato, Phys. Rev. B **81**, 060504(R) (2010).
- ⁵⁰ Y. Nagai and K. Kuroki, Phys. Rev. B **83**, 220516(R) (2011).
- ⁵¹ S. Onari and H. Kontani, arXiv:1105.6233v1. Numerical results have been improved since arXiv:1105.6233v2.
- ⁵² J. G. Checkelsky, L. Li, G. F. Chen, J. L. Luo, N. L. Wang, and N. P. Ong, arXiv:0811.4668.
- ⁵³ J. J. Tu, J. Li, W. Liu, A. Punnoose, Y. Gong, Y. H. Ren, L. J. Li, G. H. Cao, Z. A. Xu, and C. C. Homes, Phys. Rev. B **82**, 174509 (2010).
- ⁵⁴ A. S. Sefat, M. A. McGuire, B. C. Sales, R. Jin, J. Y. Howe, and D. Mandrus, Phys. Rev. B **77**, 174503 (2008).
- ⁵⁵ B. P. Stojkovic and D. Pines, Phys. Rev. B **56**, 11931 (1997).
- ⁵⁶ T. A. Maier, S. Graser, D. J. Scalapino, and P. Hirschfeld, Phys. Rev. B **79**, 134520 (2009).
- ⁵⁷ Y. Nagai and K. Kuroki, arXiv:1106.2376.
- ⁵⁸ S. Onari and H. Kontani, arXiv:1107.0748.
- ⁵⁹ H. Kadowaki, T. Sato, H. Yoshizawa, T. Ekino, T. Takabatake, H. Fujii, L. P. Regnault, and Y. Isikawa, J. Phys. Soc. Jpn. **63**, 2074 (1994).
- ⁶⁰ S. Raymond, L. P. Regnault, T. Sato, H. Kadowaki, N. Pyka, G. Nakamoto, T. Takabatake, H. Fujii, Y. Isikawa, G. Lapertot, and J. Flouquet, J. Phys. Cond. Matt. **9**, 1599 (1997).
- ⁶¹ H. Ikeda and K. Miyake, J. Phys. Soc. Jpn. **65**, 1769 (1996).
- ⁶² T. Mutou and D. S. Hirashima, J. Phys. Soc. Jpn. **64**, 4799 (1995).
- ⁶³ T. Mutou and D. S. Hirashima, J. Phys. Soc. Jpn. **63**, 4475 (1994).